

Article

Processability of High-Speed Steel by Coaxial Laser Wire Deposition Technology for Additive Remanufacturing of Cutting Tool

Piotr Koruba ^{*}, Jakub Kędzia, Robert Dziejczak  and Jacek Reiner 

Department of Laser Technologies, Automation and Production Engineering, Wrocław University of Science and Technology (WUST), Wyb. Wyspińskiego 27, 50-370 Wrocław, Poland; jakub.kedzia@pwr.edu.pl (J.K.); robert.dziejczak@pwr.edu.pl (R.D.); jacek.reiner@pwr.edu.pl (J.R.)

* Correspondence: piotr.koruba@pwr.edu.pl; Tel.: +48-71-320-4635

Featured Application: Additive remanufacturing of cutting tools on the example of flat broach by Coaxial Laser Wire Deposition technology.

Abstract: The recently introduced Coaxial Laser Wire Deposition technology can become a new promising method for remanufacturing high-complexity and expensive cutting tools (e.g., flat broach), which will have a significant impact on their service life. In addition, it is an innovative approach to tool management. An analysis of the feasibility of processing cobalt-added HSS powder steels was carried out for single clads and multilayer structures. The effect of process parameters (laser, beam power, travel speed, wire feed rate) on geometric properties, hardness and microstructure was discussed. In order to avoid cracking during multilayer deposition, an additional preheating to 320 °C was applied. Two sets of process parameters with high and low heat input were obtained. Both sets lead to crack-free structures that fulfill geometric (≥ 2.5 mm in height) and hardness (≥ 700 HV) requirements.



Citation: Koruba, P.; Kędzia, J.; Dziejczak, R.; Reiner, J. Processability of High-Speed Steel by Coaxial Laser Wire Deposition Technology for Additive Remanufacturing of Cutting Tool. *Appl. Sci.* **2023**, *13*, 11232. <https://doi.org/10.3390/app132011232>

Academic Editors: Zhenglong Lei, Xianglong Wang and Shuai Chang

Received: 13 September 2023

Revised: 9 October 2023

Accepted: 10 October 2023

Published: 12 October 2023



Copyright: © 2023 by the authors. Licensee MDPI, Basel, Switzerland. This article is an open access article distributed under the terms and conditions of the Creative Commons Attribution (CC BY) license (<https://creativecommons.org/licenses/by/4.0/>).

Keywords: additive remanufacturing; DED-LB/M; HSS; cutting tool repair; laser material processing

1. Introduction

The variety of cutting tools used in industry need to fulfill high requirements for hardness, toughness, wear resistance and exposure to elevated temperatures. High-speed steels (HSSs) meet all these requirements since they exhibit high hardness, bending strength and grindability [1]. These steels are Fe-C type with additions of Cr, W, Mo, V and Co, while they can be quenched with air cooling from austenization temperature. Their applications apart from cutting tools are forging and punching dies, injection molds, automotive components and space vehicles [2]. HSSs are characterized by high wear resistance and good mechanical properties due to the occurrence of a specific microstructure, i.e., a matrix of martensite and residual austenite with a grid of eutectic carbides uniformly distributed in interdendritic regions [3]. The presence of vanadium carbides, for example, is crucial from the point of view of the proper grindability of the produced tools [4]. In contrast, the increased content of cobalt in HSS results in the growth of resistance to loss of hardness at elevated temperatures and prevents cold cracking [5]. The majority of the cutting tools that need to meet increased strength criteria are made from HSS-Co steels, which are nowadays being produced through powder metallurgy (PM). The established manufacturing process for PM steels is complex and includes powder production, hot isostatic pressing (HIP), and forging followed by heat treatment with hardening and triple tempering [6]. This metallurgical process allows for obtaining a finer grid of carbides that also improves grindability [4]. High-alloy tool steels such as HSS-Co PM are considered non-weldable and prone to fracture. Therefore, processing them with additive manufacturing

(AM) technologies is still a challenge because of their low repeatability [1]. The use of AM to repair a tool can lead to an anisotropy of the resultative microstructure and cause different properties of the deposited structure in relation to the substrate [7]. Another issue in developing AM technology is the accumulation of expansion and contraction stresses caused by the deposition of successive layers of additional material [8].

Among many AM techniques for processing metal alloys, one can distinguish two widely used groups of technologies: direct energy deposition (DED) and powder bed fusion (PBF) [9,10]. Comparing the DED technique with PBF, it can be claimed that DED is characterized by a lower dimensional and shape accuracy but higher material deposition efficiency [11]. Although PBF usually permits obtaining better component properties, in some cases, DED allows achieving better mechanical properties and easier gradation by varying material composition [12]. Laser metal deposition (LMD) is a specific type of DED technology that can be used in the production, modification and reconditioning of machine parts, especially those with complex and expensive manufacturing processes that have to meet high requirements regarding abrasion, wear and corrosion resistance on surfaces exposed to wear and harsh conditions [9,13].

The use of a laser beam as a heat source is associated with a lower amount of heat introduced into the material and, therefore, a smaller size of the melt pool and heat-affected zone (HAZ) [11]. Moreover, when the majority of conventional welding processes are characterized by cooling rates of 10–100 K/s, at laser material processing, the cooling rates are in the range of even 1000–10,000 K/s [14].

Some significant advantages can be achieved in the LMD by feeding additional material coaxially to the laser beam, i.e., independence of material deposition from the direction of laser head movement as well as the ease of supplying the shielding gas. Admittedly, there is a possibility of using the additional material in both powder and wire form. The wire gives the possibility of achieving 100% melting efficiency and higher volumetric deposition rates [15], whereas coaxial powder feeding is much more common. The lateral wire feed method reduces flexibility and increases the difficulty of process control when manufacturing complex parts. It leads to the conclusion that the most effective technology for additive manufacturing or remanufacturing is Coaxial Laser Wire Deposition (CLWD). The wire material is fed precisely and coaxially to the axis of the optical system, which can form the shape of a laser beam using one of two methods: splitting the beam into three separate tracks and then focusing them at a single location under the wire feed nozzle or shaping a laser beam into a ring, splitting it into two half-rings by a prism, and refocusing into an annular shape [16].

On the other hand, as a result of the large angle between the wire and the modified laser beams, the process window for stable wire melting is significantly reduced compared to the lateral wire feed system. The relative position of the laser beam focus relative to the wire tip has a significant impact. In extreme cases, wire dripping or wire stubbing can occur, both of which are considered to be faulty processes [17]. According to [18], in order to achieve a defect-free process, it is necessary to determine the influence of extended process parameters such as wire and travel speed ratio and energy per unit length.

The area of applications for the CLWD process includes the deposition of functional coatings (wear protection coatings for iron, cobalt, nickel and copper alloys), remanufacturing (repair of forming tools), and additive manufacturing (fabrication of components made of titanium and nickel alloys) processes [19]. This AM technology is under development, and the results of carrying out the CLWD process for hard-weldable materials from which cutting tools are made have not yet been presented.

In the case of HSS processing with a laser beam, the effect of laser surface re-melting on the hardness of HSS was investigated with a 20–30% decrease in the hardness of ASP23 and ASP30 steels observed. Additionally, an improvement in corrosion resistance was observed by the phenomenon of dissociation and refinement of carbides [2]. Some tool steels can be favorable materials for the LMD process because they provide relatively high hardness without cracking. This is a result of the low process-induced residual stresses

caused by the favorable coefficient of thermal expansion and the volumetric expansion associated with the formation of solid martensite during cooling [20]. However, there are reports about defects revealed during the LMD of tool steels, such as porosity, cracks and a lack of fusion. The solution to avoid cracking may be to preheat the substrate so that a reduction in thermal stresses is possible [13]. In [21], a preheating temperature of 150 °C was used in the process of HSS coating deposition, which allowed holding the material at an equilibrium temperature close to the martensite start temperature and resulted in the absence of cracking. Another example of heat treatment after the LMD process of M2 steel on the substrate of AISI 1045 steel was the additional 2 h of tempering at 550 °C [3]. It is also worth mentioning that during the multilayer deposition of HSS coatings, the phenomenon of tempering of previous clads was observed, but the addition of cobalt in the steel may result in a lesser tempering effect [21]. Moreover, during an extended study of the LMD process of HSS alloys with variable V content, the observed microstructure of the received clads was highly fine-grained compared to conventional casting processes due to the high cooling rates. The shape of VC carbides corresponded with the microhardness of the clad and was highly dependent on the travel speed parameter, while the size of VC carbides influenced the resistance to high-temperature wear phenomena [22]. LMD technology was also used to create a chip-breaking dot on a lathe knife made of W6Mo5Cr4V2 steel with the aim of modifying the functionality of the tool edge by shaping the chip and increasing the service life of the tool [23].

This paper presents the results of developing novel Coaxial Laser Wire Deposition technology for the processing of high-speed steels. The complex analysis of the processing possibilities of cobalt-added HSS powder steels allows an assessment of the applicability of this technology in the additive remanufacturing of cutting tools. The research carried out consists of technological tests for single clads and multilayer structures. The obtained geometrical parameters of the deposited structures were analyzed from the point of view of the dimensional and shape reproducibility of an example of a shaping cutting tool—a toothed bar or flat broach. Moreover, the hardness of the clad and the heat-affected zone received in the CLWD process were analyzed in relation to the used process parameters. The analysis of deposition results also included microstructure examination using optical and SEM methods. Due to the difficulty of obtaining crack-free multilayer structures, additional preheating of the substrate material to temperature above the martensitic transformation start temperature (M_s) was used, allowing two sets of process parameters to be determined: an efficient set and one low-heat input set.

2. Materials and Methods

2.1. Materials

An exemplary cutting tool, which is the subject of an analysis on the feasibility of remanufacturing in the CLWD process, is shown in Figure 1a. It is assumed that damage to the tool will require the removal of a single row of teeth followed by the deposition of the additional material and the reconstruction of the overall geometry according to Figure 1b. These assumptions define the required height of the deposited material to be a minimum of 2.5 mm. However, due to the laser spot size, which is larger than the overall width of the tooth, the issue of obtaining the appropriate clad width should not be a challenge.

Experimental tests of the CLWD process were carried out on the BÖHLER S390PM substrate, which is the commercial equivalent of the steel mentioned in the norm [24]. The samples for the tests were prepared in the form of plates with dimensions of 200 mm × 40 mm × 15 mm by waterjet cutting and surface sandblasting. The substrate material was manufactured by powder metallurgy to a hardened state and subsequently tempered three times after hot forging. The microstructure of fine-grained martensite with 32% uniformly distributed carbides without residual austenite is observed (Figure 2). During the Scanning Electron Microscopy (SEM) analysis, the primary and secondary carbides were identified within the matrix. The presence of carbide-forming elements was also analyzed by the Energy-Dispersive Spectroscopy (EDS) method, showing the distribution of vanadium,

molybdenum, tungsten, and chromium in the sample (Figure 2). The average measured hardness value was 805 ± 30 HV1. Based on the CCT diagram provided by the material manufacturer, the value of the Ms temperature is about $300\text{ }^{\circ}\text{C}$ [25].

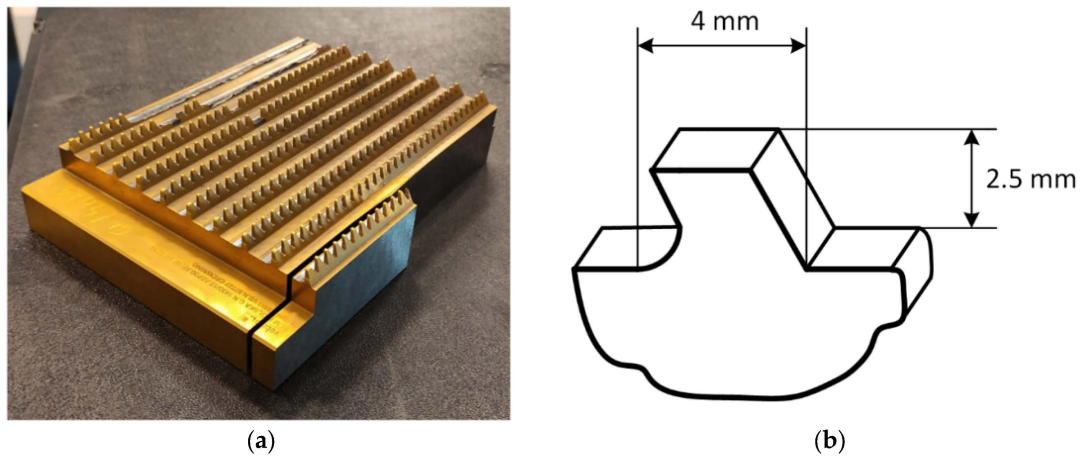


Figure 1. Object of the planned remanufacturing—broach cutting tool: (a) photo of a broach fragment, (b) close-up of a single tooth with overall dimensions.

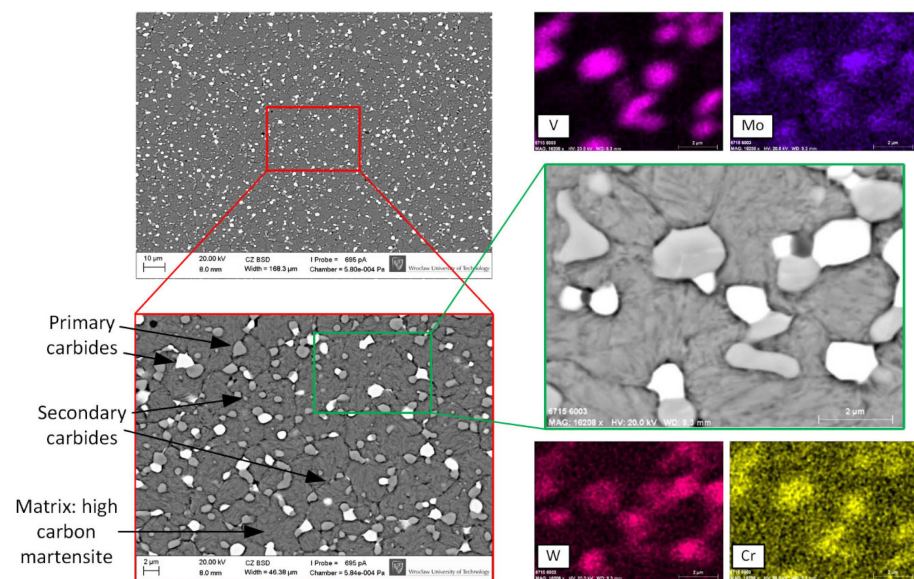


Figure 2. SEM microstructure of the cutting tool substrate material with different magnification factors showing the distribution of primary and secondary carbides formed during the S390PM steel manufacturing process. The distribution of carbide-forming elements was also visualized using EDS analysis.

Additional material in the process was LAWI 64 wire with a 0.6 mm diameter that was copper plated. During the SEM analysis of the wire material, the lack of integrity of the copper coating was observed (Figure 3). This resulted in the presence of oxygen in the additional material transferred to the melt pool during the process, which can increase the risk of porosity as a result of the high affinity of carbon for oxygen.

In order to determine the chemical composition of both the substrate and the wire materials, the EDS method was used during the SEM analysis. The chemical composition of the materials is shown in Table 1.

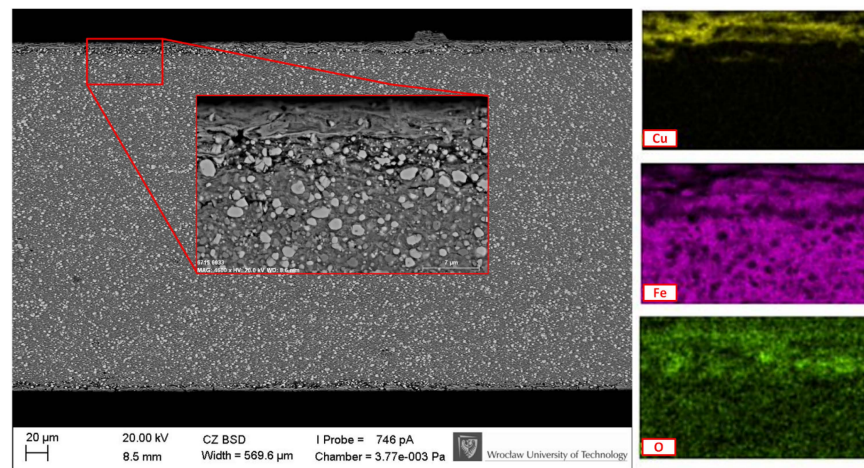


Figure 3. Analysis of the additional wire material: a general view of the microstructure with a magnification on the copper-coated surface layer and EDS analysis results for iron, copper and oxygen.

Table 1. Chemical compositions of substrate and wire materials obtained using the EBDS technique.

Material	Chemical Composition (%)									
	Fe	C	W	Co	Cr	V	Mo	Si	Mn	
BÖHLER S390PM	bal.	1.62	9.98	7.47	4.91	4.35	1.85	0.43	0.29	
LAWI 64	bal.	1.07	4.04	-	3.74	2.0	10.67	-	-	

Specimens fabricated during the CLWD process for metallographic analysis were prepared using a metallographic cutter with diamond cut-off wheels. Subsequently, they were mounted, grinded, polished, and etched with 5% Nital. The geometric properties of the clad were measured with the VHX-600 digital microscope (Keyence, Osaka, Japan). Microstructure analysis was carried out with the use of the LEXT OLS4000 (Olympus, Tokyo, Japan) and the ZEISS SIGMA 500VP (ZEISS, Jena, Germany). microscopes Microhardness tests were performed on the Zwick–Roell ZHV μ -A device. Measurements were made with a load of 1 kG using the Vickers method. Indentations were made on the cross-section of the clad along its axis with a constant spacing of 300 μ m.

2.2. Experimental Setup

Experimental studies of CLWD technology were carried out on a laser metal deposition station equipped with a 4 kW HPDL laser unit (Laserline 4000-30). The laser beam was delivered by an optical fiber with a core diameter of 600 μ m to the COAXwire M process head (Coaxworks GmbH, Dresden, Germany), which was characterized by a focal length of collimating and focusing optics of 100 mm and 300 mm, respectively. The optical system of the COAXwire M divides the laser beam into three separate optical paths. The resulting beams are directed at an angle of 20° to the normal of the substrate material, allowing the coaxial insertion of additional wire material (Figure 4a,b). The power distributions of the laser beam were measured at several planes near the focus using the FocusMonitor device (PRIMES GmbH, Pfungstadt, Germany). The results of the measurements are shown in Figure 4c. Due to the folding of the three laser beams at the processing point, the working distance relative to the position of the laser beam focus was defined as ± 2 mm. The movement of the processing head was provided by the Reis RV60-40 6-axis robot (Figure 4d). The wire was supplied by the Dinse FD 100 LS-WB wire feeder, providing feeding up to 7 m/min. A constant flow of shielding gas (Ar) was ensured by the Vögtlin GSC-C9SA gas flow controller. The preheating of the substrate was provided by the high-temperature titanium hot plate PZ 28-3T (PRÄZITHERM). The preheating temperature was monitored by a set of thermocouples at different locations in the samples.

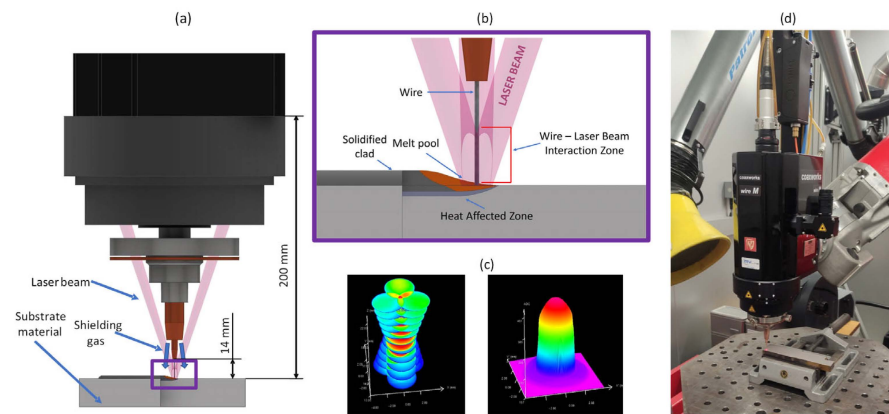


Figure 4. Applied stand for the CLWD process: (a) idealized schematic diagram of the process, (b) interaction zone of the laser beam with the additional material, (c) distribution of the laser beam intensity for the COAXworks M head (3D view and 2D view for the working point), (d) view of the COAXworks M laser head on the Reis RV 60-40 robot.

The methodology for developing the additive remanufacturing technology of cutting tool geometry, using the example of a row of teeth in a flat broach, is shown schematically in Figure 5. The deposited structure obtained with the CLWD process had to meet the geometric requirements (height greater than 2.5 mm and width greater than 4 mm), hardness (higher than 700 HV), and quality (no cracks) requirements. The conducted research can be divided into four main stages: the deposition of single clads, the deposition of multiple layers to obtain the appropriate height of the structure, the application of substrate preheating for selected process parameter sets to avoid cracks, and the deposition of geometrical structures that are prefabricated for the grinding process to reproduce the geometry of the cutting tool. In the study, visual evaluation, Vickers (HV1) hardness measurements, and SEM microstructure examination were used for a comparative analysis and final verification of the developed process parameter sets.

The experimental plan developed for single clad deposition concerned three process parameters: laser power, travel speed and wire feed rate. The remaining process parameters, i.e., focus position, amount of shielding gas, and free wire length, were kept constant (Table 2). The wire feed rate coefficient (WFRC) that is present in Table 2 is defined as the ratio of wire feed rate to travel speed. The length of the deposited track was 30 mm for the single clad process and 50 mm for multilayer deposition. The number of layers was derived from the geometrical requirements for the remanufactured element and resulted from the particular parameter set. In the second part of the study, the initial conditions of the process were established by preheating the substrate material at a temperature T_0 of 320 °C.

Table 2. Sets of process parameters used for the first phase of the study—deposition of the single clads.

Parameter Set No.	Laser Power (W)	Travel Speed (mm/s)	Wire Feed Rate (mm/s)	WFRC	Laser Spot Diameter (mm)	Shielding Gas Flow (L/min)	Free Wire Length (mm)
1	2000	5	60	12	4.5	20	14
2			70	14			
3			80	16			
4	2500	10	80	8			
5			100	10			
6			117	11.7			
7	2500	15	60	4			
8			90	6			
9			117	7.8			

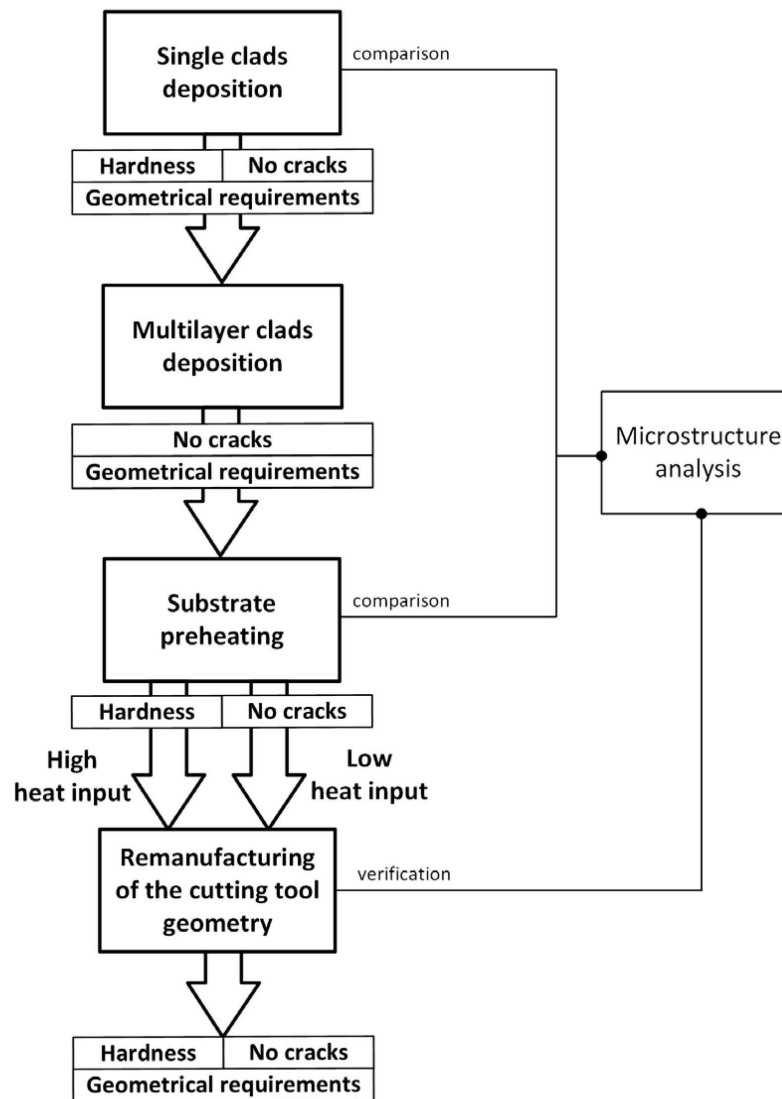


Figure 5. Schematic of the research methodology for the development of additive regeneration technology for the HSS-Co PM cutting tools using the CLWD process.

3. Results and Discussion

3.1. Geometrical Analysis

Firstly, the received single clads were subjected to a visual assessment in order to select the appropriate technological parameters. The visual analysis indicated the presence of macrocracks in samples no. 2 and 3 (Figure 6). According to [26], the cracking of the HSS material during DED can be due to hot or cold cracking. The microstructure analysis did not show the occurrence of microcracks at prior austenite grain boundaries, which is typical for hot cracks in this kind of material. In contrast, macrocracks in the heat-affected zone are a characteristic representation of cold cracking in the DED process. This may be a result of the relatively high residual stresses caused by the rapid solidification of a significant amount of material. The susceptibility to cracking is additionally increased by the high carbon content in processed materials and an unfavorable cladding structure that results in geometric notches. On this basis, these two sets of parameters were excluded from further studies. Despite the absence of cracks for the remaining seven sets of parameters for single clads, the geometric requirement (clad height ≥ 2.5 mm) was not met (Figure 7a). Therefore, there was a necessity for the multilayer CLWD process to achieve this requirement.

The clad height increases with the wire feed rate, whereas it decreases as the travel speed rises. This enables one to determine the dependence between the clad height and the WFRC parameter, which is shown in Figure 7c. A linear correlation with a high R^2 value (> 0.99) was found. Regardless of the set of parameters used, the width of the clad remains at the same level (Figure 7b). Furthermore, the minimal requirement for the width of the remanufactured clad was fulfilled (>4.0 mm). It can be concluded that for a WFRC coefficient higher than 14, cracking can occur.

One of the important factors in the process of multilayer laser metal deposition is the strategy of material deposition. It can allow one to avoid the stress concentration caused by the nonuniform build-up of successive layers. Therefore, subsequent clads were deposited with laser beam movement in opposite directions. The use of the mentioned approach may allow for a uniform geometry of the clad along its length and a resulting more beneficial stress distribution. Figure 8 shows the results of the multilayer CLWD process considering the number of layers, their gradual height, and the occurrence of cracks. As the number of layers increases, a significant decrease in the quality of the deposited structures can be observed, as revealed by the presence of cracks. Only for the parameter set with the highest travel speed and the lowest wire feed rate (no. 7), a crack-free two-layer structure was obtained. It can be observed that for the eighth and ninth parameter sets, cracking occurred for two-layer structures, while the clad heights for these trials have been close to the height of the single crack-free clad no. 1. This suggests an increased contribution of residual stresses to the crack formation process for the two-layer deposition process.

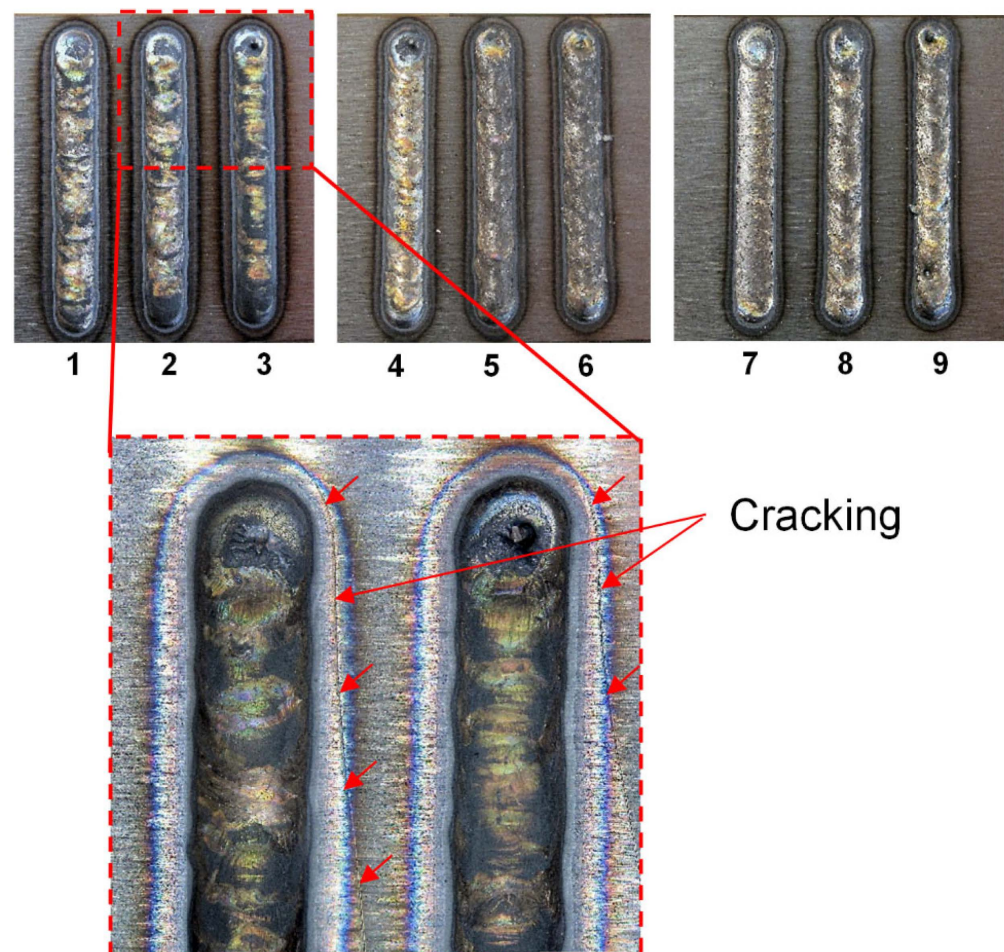


Figure 6. A view of the deposited single clads with 9 different sets of process parameters.

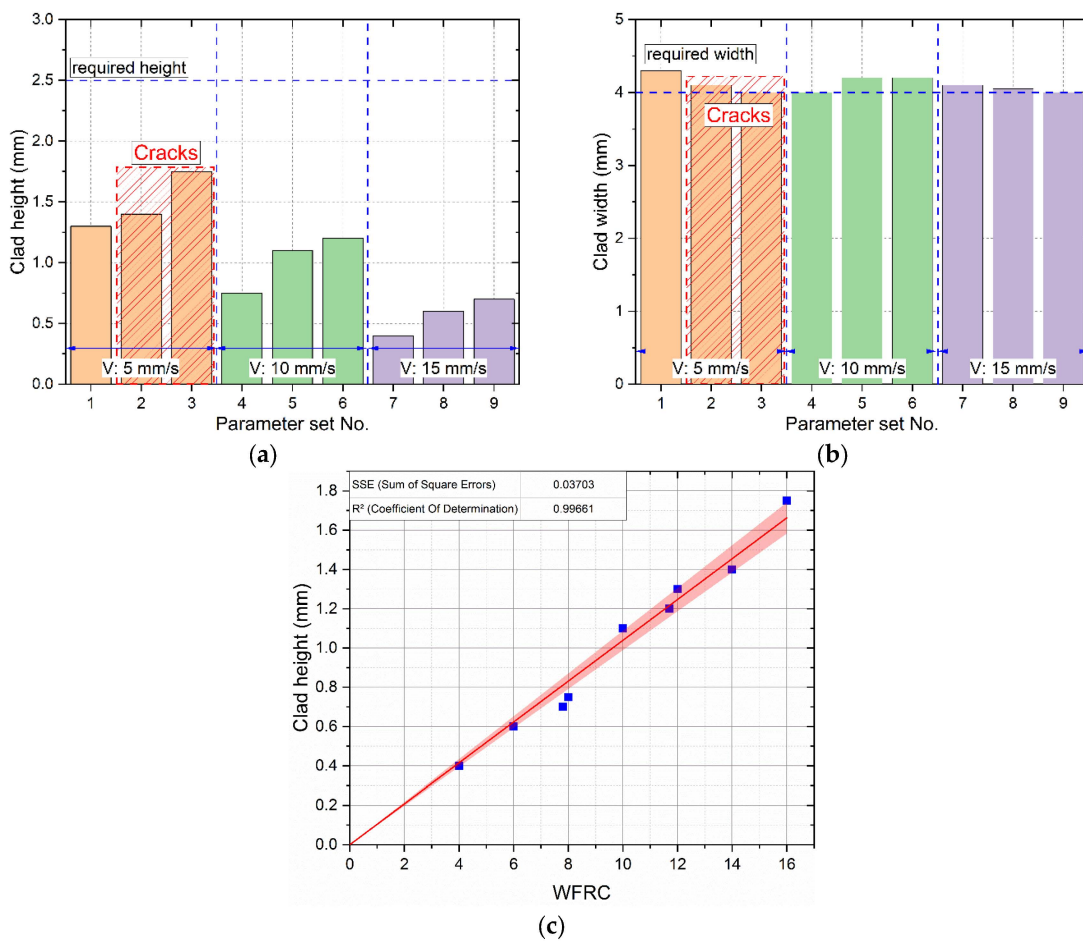


Figure 7. Results of measurements of geometrical properties of single clads with different parameter sets: (a) results of the clad height measurement, (b) results of the clad width measurement, (c) linear correlation between the clad height and the complex process parameter.

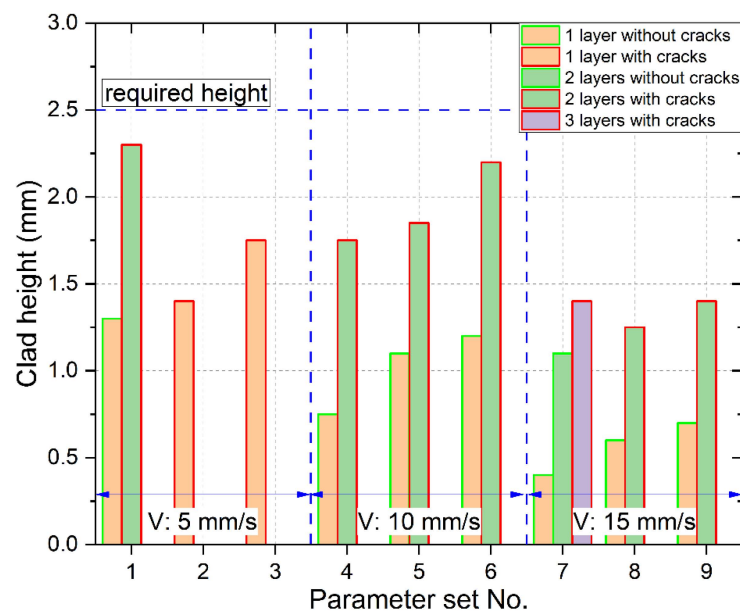


Figure 8. Results of the deposition of multilayer clad structures—clad heights obtained for the deposition of 1, 2 or 3 layers of additional material.

As stated in the previous paragraph, during the continuous cooling of the S390PM material, the Ms temperature does not exceed 300 °C. Keeping the material above this temperature during the deposition of subsequent layers can lead to a reduction in stress level resulting from the phase transformation and allow obtaining the state of compression in the clad. Furthermore, preheating the substrate allows for decreasing temperature gradient during cooling, overcoming the risk of cracking that was observed during CLWD trials carried out at room temperature for single and multilayer clads.

In order to achieve uniform preheating of the substrate material and the certainty of exceeding the Ms temperature, the preheating temperature value was set at 320 °C. Preheating tests were conducted for two boundary values of travel speed, i.e., 5 mm/s and 15 mm/s, with the same wire feed rate of 60 mm/s, which refers to the 1st and 7th parameter sets, which were defined as high and low heat input processes. This selection was motivated by differences in microstructure and the lowest susceptibility to cracking without preheating. The use of the lowest wire feed rate also decreased the probability of cracking by reducing the volume of shrunken material.

Figure 9 shows the number of layers required to achieve the required clad height of 2.5 mm. For the 5-mm/s travel speed, only three subsequent passes were required, while for the speed of 15 mm/s, the value of passes increased to 8. The reason for this situation is the volume of wire material during subsequent passes. During the high heat input process, 170 mm³ of additional material was used for a single clad deposition, where for a lower heat input, this value dropped by 66%. Based on theoretical calculations of the volume of fed material, assuming 100% of its utilization, the resultative difference of the deposited material should be about 12%. However, the results of the cross-sectional area measurements of the clads show a different value of 40%, which results from the variable size of the melt pool during processing and the presence of spatters (Figure 9). Visual and microstructural investigations of the samples after self-cooling (2 h) showed the lack of cracks in the deposited structures.

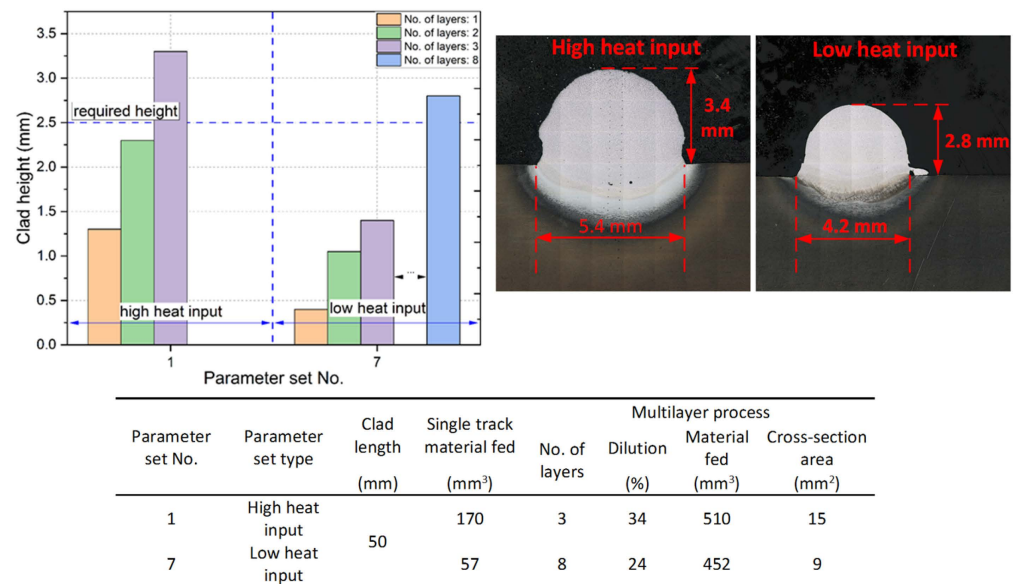


Figure 9. Results of clad height measurement for 2 selected sets of process parameters: efficient set and low heat input set.

3.2. Microstructure Investigation

For easier analysis of the results, all microstructure images shown in this section (Figures 10 and 11) were acquired at the same magnification.

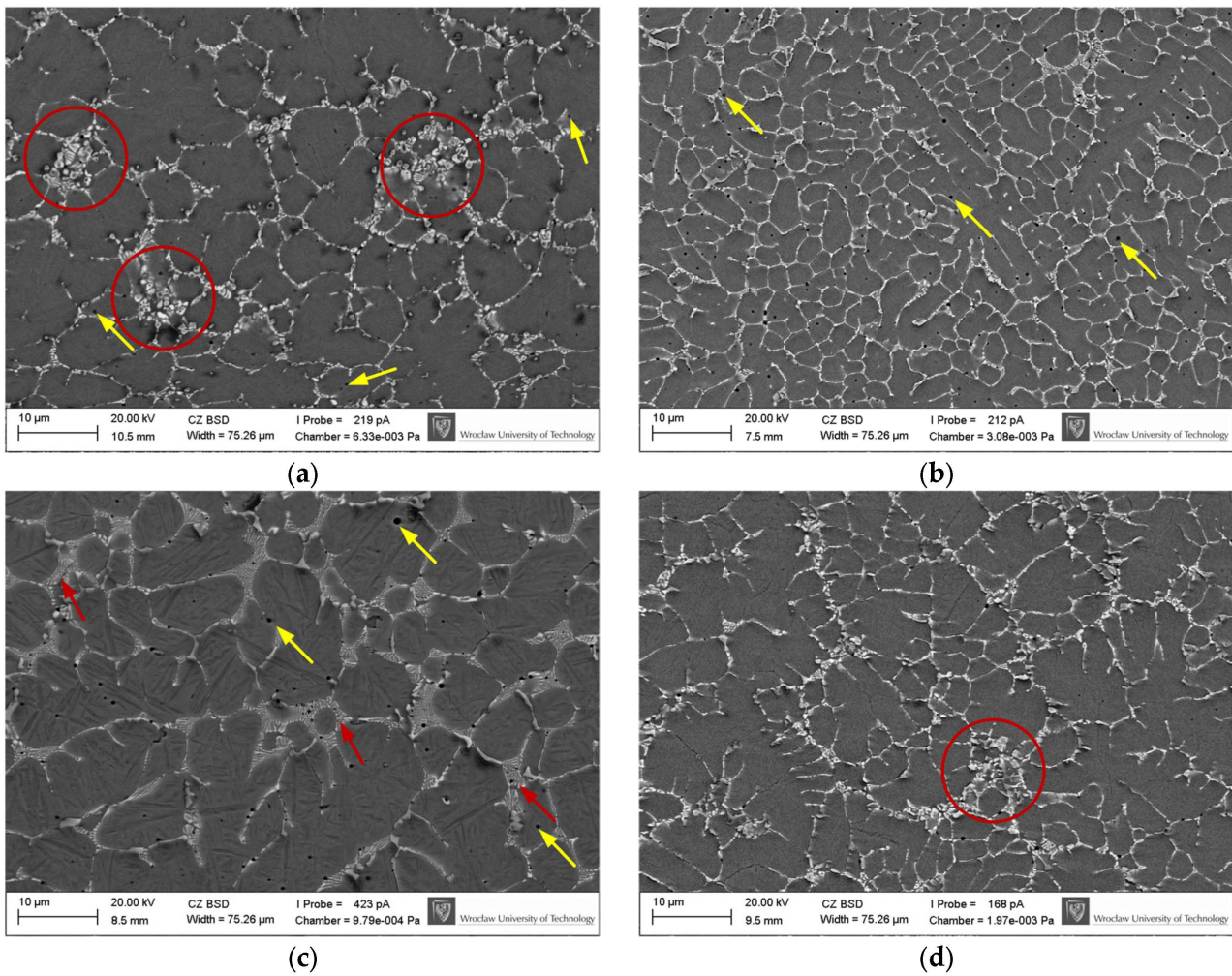


Figure 10. SEM microstructure of single clads deposited with selected sets of process parameters: (a) set No. 1, without preheating (T_0 : 0 °C), (b) set No. 7 without preheating (T_0 : 0 °C), (c) set No. 1 with preheating (T_0 : 320 °C), (d) set No. 7 with preheating (T_0 : 320 °C).

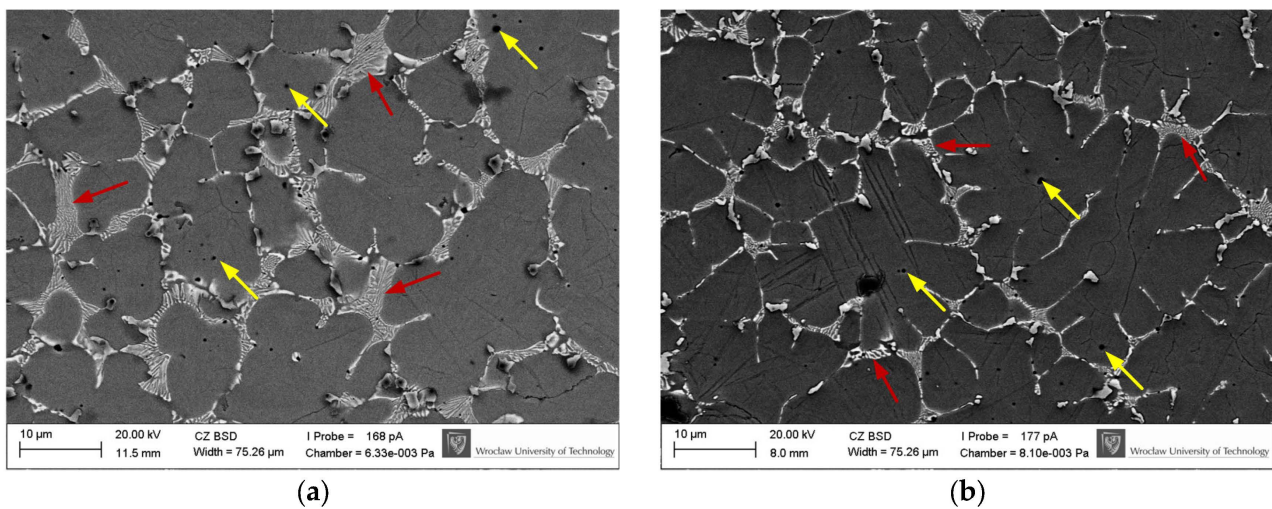


Figure 11. SEM microstructure of multilayer structures with preheating (T_0 : 320 °C): (a) Number of layers: 3, parameter set No. 1, (b) Number. of layers: 8, parameter set No. 7.

The microstructure analysis of single clads demonstrated significant differences for extreme process travel speeds: 5 mm/s and 15 mm/s (Figure 10a,b). In Figure 10a, two types of carbides were observed: the first is a discontinuous grid of carbides formed from melting and solidification, while the second shape is partially melted carbides that form clusters (red circles). On the sample prepared with a lower travel speed (Figure 10a), a discontinuous grid of carbides has formed at the prior austenite grain boundaries, but there are also areas without carbides visible. A little gas porosity can also be detected (yellow arrows). In contrast, for a higher travel speed (Figure 10b), a finer continuous grid of carbides was observed. In a much greater degree (compared to the lower travel speed), the grid of carbides formed at the boundaries of prior austenite grain boundaries. Due to the higher travel speed, the structure clearly shows areas with dendritic regions. In this sample, the highest number of small gas pores is present (yellow arrows). Moreover, the lack of carbide clusters indicates the complete dissolution of carbides during the melting of additional material. X-ray diffraction examination showed that the clad structure consists solely of martensite and carbides. No residual austenite was detected. The coarser microstructure in Figure 10a is the result of higher heat input compared to Figure 10b, in which the presence of fine dendrites was identified.

Further investigations consisted of an analysis of the effect of preheating on the microstructure obtained for the clads (Figure 10c,d). Preheating for a lower travel speed caused the growth of matrix grains and thickening of the carbide grid, which was perceived as an eutectic-like structure (Figure 10c, red arrows). In comparison to the sample without preheating the substrate, no clusters of unmelted carbides were observed. A few little gas pores are visible (yellow arrows). However, for a higher travel speed (Figure 10d), a slightly finer microstructure was received, resulting in a considerably thinner grid of carbides with only one potential cluster (red circle). The presence of dendrites in the microstructure was preserved. In both cases, the martensitic structure is clearly visible. In this case, no gas pores were found (yellow arrows). Due to their submicrosize and number, the presence of micropores should not be an issue in ensuring the functional properties of remanufactured cutting tools, i.e., hardness.

The CLWD multilayer process with high heat input leads to a microstructure similar to that obtained for single clads (Figure 10c). The only differences are a slightly larger structure and thicker eutectic precipitations (Figure 11a, red arrows). On the other hand, the low heat input process (Figure 11b) delivers a coarser dendritic structure compared to Figure 10d. In both samples, several micropores were detected (yellow arrows). Generally, the multilayer processes in both cases caused a change in the thermodynamic conditions, which resulted in an increase in the solidification time and growth of the obtained structures.

In Figure 12, two XRD patterns were presented: red from the substrate and blue from the clad. In both cases, the highest peaks come from martensite. In the substrate material, two types of carbides were identified: MC and M₆C. In the clad, the MC carbide was not detected, whereas for the M₆C carbide, the intensity of the diffraction peaks is significantly lower than for the substrate material. This is partially a result of a lower carbon content in the additional wire material and a higher degree of carbon dissolution in the martensite.

3.3. Hardness Tests

Figure 13 shows the Vickers hardness profiles measured for samples fabricated with the parameters shown in Table 2. Through analysis of the results received, it can be observed that the average hardness value for the upper part of the clads deposited at a travel speed of 5 mm/s (768 HV₁) is about 6–7% lower than for travel speeds of 10 and 15 mm/s (817 and 825 HV₁, respectively). The reason for this phenomenon is that a much lower cooling rate is obtained for the slowest deposited clads, whereas for higher travel speeds, the cooling conditions remain relatively similar.

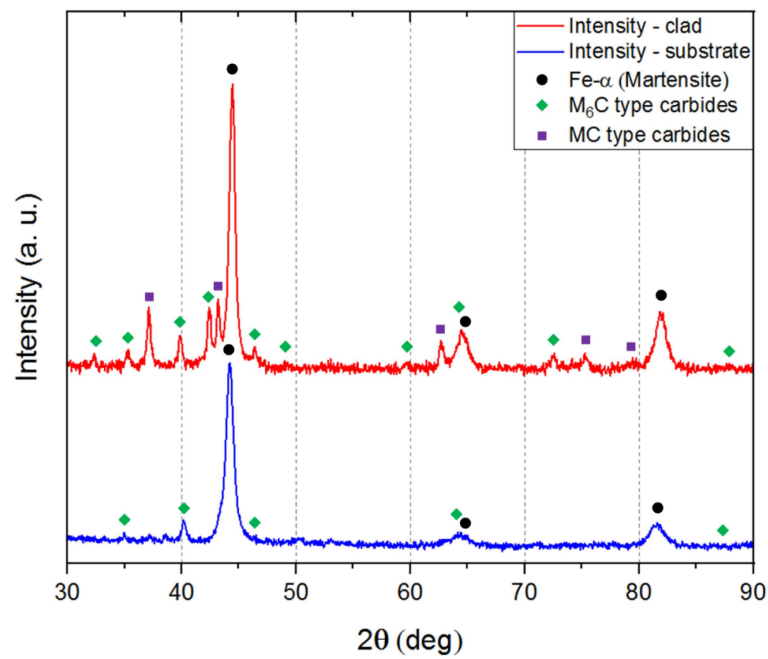


Figure 12. XRD pattern received for samples of substrate material and the clad.

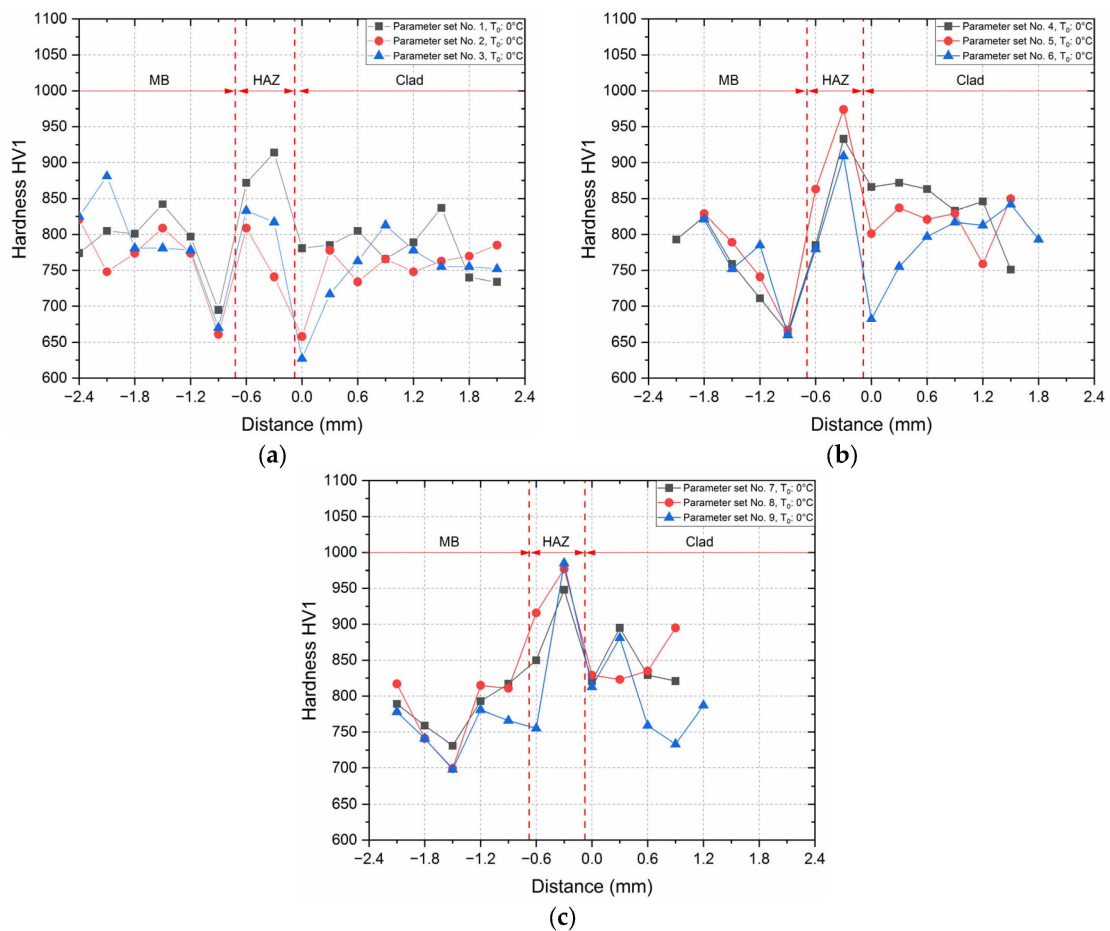


Figure 13. Results of the hardness measurement for single clads with the specifying substrate, heat-affected and clad zones: (a) parameters sets 1 to 3 (travel speed: 5 mm/s), (b) parameters sets 4 to 6 (travel speed: 10 mm/s), (c) parameters sets 7 to 9 (travel speed: 15 mm/s).

Upon a deeper analysis of the hardness profiles, it is possible to notice two areas of a significant decrease in the hardness value for certain process conditions. The first drop can be observed at the boundary of the clad and HAZ for travel speeds of 5 and 10 mm/s. This is due to the relatively low cooling rate, which is affected by the increase in the volume of additional material. This decrease is proportional to the wire feed rate and is inversely proportional to the travel speed. As a result, this phenomenon cannot be noticed at the highest travel speed of 15 mm/s, where similar solidification conditions of the clads were maintained. The visual evaluation of the clads carried out previously showed the presence of cracks in the samples fabricated with the lowest travel speed and higher wire feed rates. It can be pointed out that crack initiation may occur in the HAZ or its boundaries. Analysis of the hardness profile shows that directly in the HAZ, there are the greatest fluctuations in hardness, structure and residual stresses. Another important factor was the increase in the geometric notches that appeared as the amount of additional material increased. Fracture did not occur with higher process speeds due to a lower decrease in hardness value in this area. Moreover, the smaller volume of the deposited material reduced the shrinkage that contributes to cracking. The second drop located just below the HAZ is the result of tempering the substrate material that has not reached the austenitizing temperature during the process. However, the clads deposited with the highest travel speed again do not indicate the mentioned decrease in the hardness value because of the lower amount of heat introduced to the substrate material.

In the HAZ itself, one can also notice a local maximum of hardness located in the area that had the highest heat dissipation rate during cooling from the austenitizing temperature, resulting in the hardening of this area. The maximum hardness value increases with the speed of the process. For the two lowest travel speeds, the value of the mentioned peak hardness slightly decreases as the wire feed rate increases.

The effect of preheating on the distribution of the hardness profile of the clad was also analyzed for two extreme travel speeds (Figure 14). In both cases, the resultant hardness of the clads did not change significantly. In the HAZ, a decrease in the peak hardness of about $50 \div 60$ HV was observed due to the reduced temperature gradient. In the case of the area of the substrate material, preheating causes an increase (Figure 14a) or appearance (Figure 14b) of the tempered zone. The received width of this zone is larger for a lower travel speed due to the higher heat input.

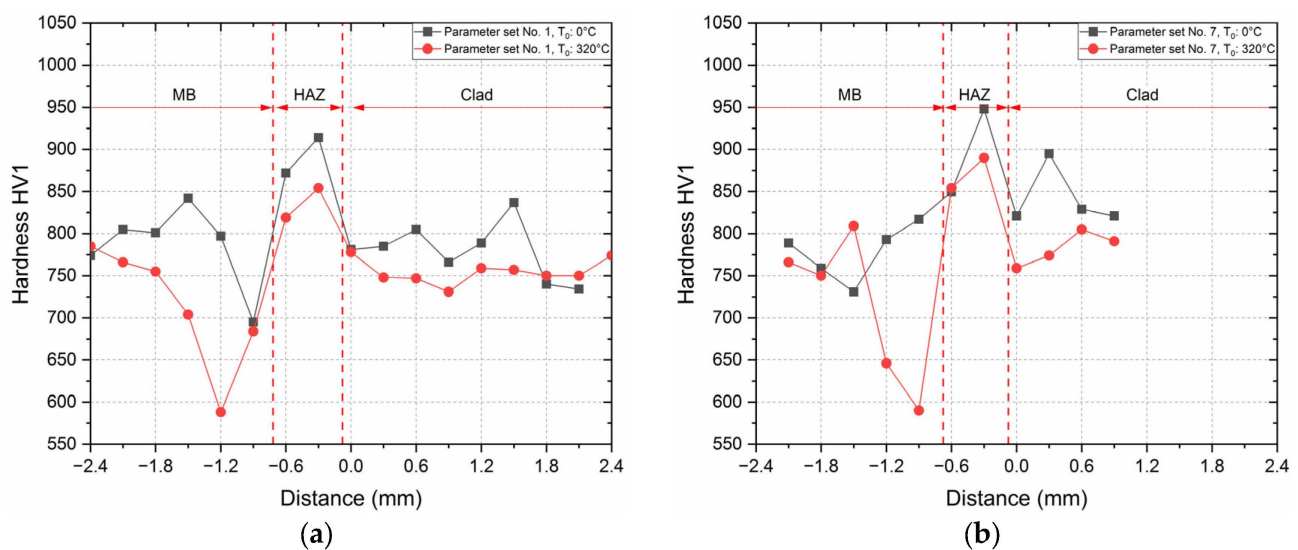


Figure 14. Results of hardness measurement for single clads with selected parameters sets with high and low heat input. Comparison of the result with/without additional preheating (T_0 : 320 °C): (a) parameter set No. 1—high heat input, (b) parameter set No. 7.—low heat input.

The result of the hardness profile measurement for the multilayer deposited structure is shown in Figure 15. The hardness of both multilayer clads is comparable: 791 HV1 (high heat input) and 797 HV1 (low heat input). Multiple thermal treatments have a positive effect on the HAZ due to its tempering and reduction in residual stresses (Figure 15b). This is revealed as a hardness drop of about 150 HV to a level comparable to the clad and substrate material. The triple passage with a lower travel speed caused a higher heat input that resulted in an increase in the width of the tempered zone in the substrate material with a dramatic drop in the hardness value.

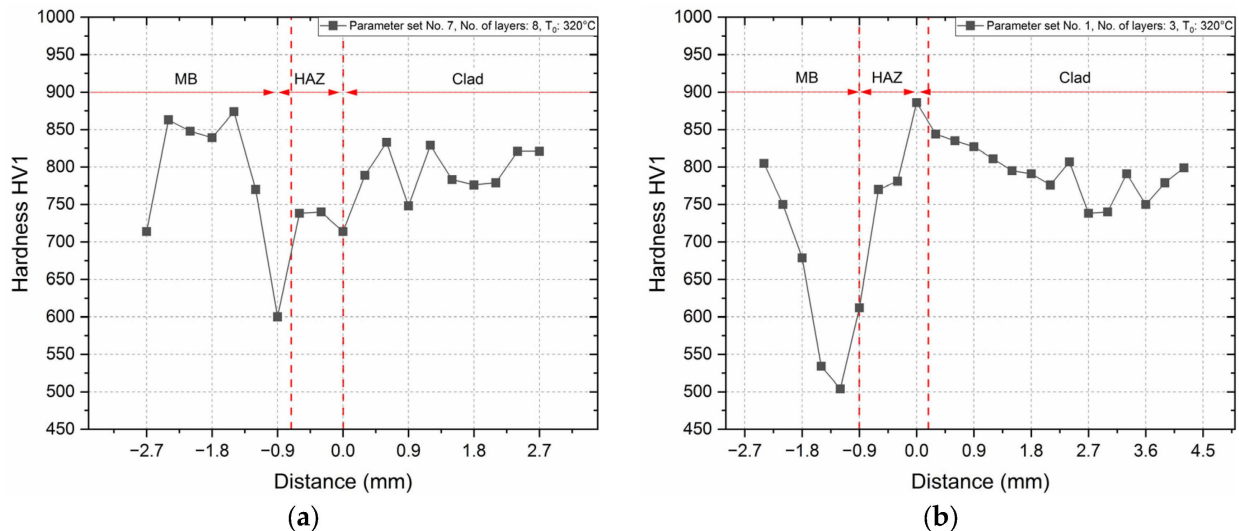


Figure 15. Results of hardness measurement for multilayer structures deposited with preheating (T_0 : 320 °C): (a) parameter set No. 1—high heat input (3 layers), (b) parameter set No. 7.—low heat input (8 layers).

4. Conclusions

As a result of research on newly developed CLWD technology for advanced use in the additive remanufacturing of cutting tools made of hard-weldable high-speed steels, two sets of process parameters were developed, i.e., low and high heat input sets. Deposited structures that met the qualitative (no cracks) and geometrical requirements based on the dimensions of the row of teeth of the tool under consideration (the broach) were obtained.

1. Single clads deposited without preheating are susceptible to cracking because of two negative factors, i.e., softening of the material at the HAZ boundaries and high shrinkage stresses induced by the relatively large size of the solidifying material. Furthermore, the accumulation of stresses in the multilayer process results in cracking for all tested sets of process parameters.
2. The average hardness of the deposited single clad at the high heat input is 6 to 7% lower than the one obtained for low heat input. Both results are comparable to the hardness of the substrate material.
3. Applying preheating to the temperature above M_s (320 °C), it is possible to obtain multilayer deposited structures over 2.5 mm in height that are crack-free.
4. Processing with a higher travel speed allows for achieving a finer continuous grid of carbides without clusters as well as a fine dendrite microstructure of the matrix. This microstructure is more beneficial in terms of the considered application.
5. Preheating of the substrate material leads to thickening of the carbide grid and the growth of matrix grains. This also affects the widening of the softening zone in the substrate material.
6. The multilayer CLWD process with lower heat input has a positive effect on the HAZ by reducing its maximum hardness value. Additionally, the tempered zone in the substrate material is narrower than in the case of a higher heat input multilayer process.

However, the technology presented in this article concerns the first stage of remanufacturing, i.e., the additive deposition of an appropriate volume of material in order to reproduce the geometry of cutting tools. The newly developed CLWD technology allows the approximate shape of the flat broach teeth to be regenerated, accepting a grinding allowance. In order to fully qualify the innovative tool reconditioning method, it is necessary to carry out grindability tests and functional tests of remanufactured tools.

Author Contributions: Conceptualization, J.R. and J.K.; methodology, P.K. and J.K.; software, P.K.; validation, P.K., J.K. and R.D.; formal analysis, J.K. and R.D.; investigation, P.K. and R.D.; resources, P.K. and J.R.; data curation, J.K.; writing—original draft preparation, P.K.; writing—review and editing, J.K. and J.R.; visualization, P.K. and J.K.; supervision, J.R.; project administration, P.K. and J.R.; funding acquisition, P.K. and J.R. All authors have read and agreed to the published version of the manuscript.

Funding: The work presented in this publication was carried out within the project “Excellence Initiative—Research University” (Polish acronym IDUB), budget number 8211204601, task “Development of a system for coaxial hot filament laser deposition with the use of additional heat sources”.

Institutional Review Board Statement: Not applicable.

Informed Consent Statement: Not applicable.

Data Availability Statement: The data during the research are available from the corresponding author on reasonable request.

Acknowledgments: The technological partner of the research was TCM Poland Tool Consulting & Management LLC, Polkowice, Poland.

Conflicts of Interest: The authors declare no conflict of interest. The funders had no role in the design of the study; in the collection, analyses, or interpretation of data; in the writing of the manuscript; or in the decision to publish the results.

References

1. Bergmueller, S.; Kaserer, L.; Fuchs, L.; Braun, J.; Weinberger, N.; Letofsky-Papst, I.; Leichtfried, G. Crack-free in situ heat-treated high-alloy tool steel processed via laser powder bed fusion: Microstructure and mechanical properties. *Heliyon* **2022**, *8*, e10171. [[CrossRef](#)]
2. Kwok, C.T.; Cheng, F.T.; Man, H.C. Microstructure and corrosion behavior of laser surface-melted high-speed steels. *Surf. Coat. Technol.* **2007**, *202*, 336–348. [[CrossRef](#)]
3. Candel, J.J.; Franconetti, P.; Amigó, V. Study of the solidification of M2 high speed steel Laser Cladding coatings. *Revmetal* **2013**, *49*, 369–377. [[CrossRef](#)]
4. Badger, J. Grindability of Conventionally Produced and Powder-Metallurgy High-Speed Steel. *CIRP Ann.* **2007**, *56*, 353–356. [[CrossRef](#)]
5. Platl, J.; Bodner, S.; Hofer, C.; Landefeld, A.; Leitner, H.; Turk, C.; Nielsen, M.-A.; Demir, A.G.; Previtali, B.; Keckes, J.; et al. Cracking mechanism in a laser powder bed fused cold-work tool steel: The role of residual stresses, microstructure and local elemental concentrations. *Acta Mater.* **2022**, *225*, 117570. [[CrossRef](#)]
6. Vogelpoth, A.; Saewe, J.; Krull, H.-G.; Richert, S.; Weiland, P.; Nerzak, T.; Eibl, F.; Pastors, F. Additive Manufacturing of Tool Steels. *Steel Res. Int.* **2023**, *94*, 2200372. [[CrossRef](#)]
7. Kok, Y.; Tan, X.P.; Wang, P.; Nai, M.L.S.; Loh, N.H.; Liu, E.; Tor, S.B. Anisotropy and heterogeneity of microstructure and mechanical properties in metal additive manufacturing: A critical review. *Mater. Des.* **2018**, *139*, 565–586. [[CrossRef](#)]
8. Shang, C.; Wu, H.; Pan, G.; Zhu, J.; Wang, S.; Wu, G.; Gao, J.; Liu, Z.; Li, R.; Mao, X. The Characteristic Microstructures and Properties of Steel-Based Alloy via Additive Manufacturing. *Materials* **2023**, *16*, 2696. [[CrossRef](#)]
9. Mahmood, M.; Bănică, A.; Ristoscu, C.; Becherescu, N.; Mihăilescu, I. Laser Coatings via State-of-the-Art Additive Manufacturing: A Review. *Coatings* **2021**, *11*, 296. [[CrossRef](#)]
10. Schneider-Maunoury, C.; Weiss, L.; Acquier, P.; Boisselier, D.; Laheurte, P. Functionally graded Ti6Al4V-Mo alloy manufactured with DED-CLAD® process. *Addit. Manuf.* **2017**, *17*, 55–66. [[CrossRef](#)]
11. Odermatt, A.E.; Dorn, F.; Ventzke, V.; Kashaev, N. Coaxial laser directed energy deposition with wire of thin-walled duplex stainless steel parts: Process discontinuities and their impact on the mechanical properties. *CIRP J. Manuf. Sci. Technol.* **2022**, *37*, 443–453. [[CrossRef](#)]
12. Sun, G.; Bhattacharya, S.; Dinda, G.P.; Dasgupta, A.; Mazumder, J. Microstructure evolution during laser-aided direct metal deposition of alloy tool steel. *Scr. Mater.* **2011**, *64*, 454–457. [[CrossRef](#)]

13. Yuan, M.; Karamchedu, S.; Fan, Y.; Liu, L.; Nyborg, L.; Cao, Y. Study of defects in directed energy deposited Vanadis 4 Extra tool steel. *J. Manuf. Process.* **2022**, *76*, 419–427. [[CrossRef](#)]
14. Bohlen, A.; Freiße, H.; Hunkel, M.; Vollertsen, F. Additive manufacturing of tool steel by laser metal deposition. *Procedia CIRP* **2018**, *74*, 192–195. [[CrossRef](#)]
15. Henri, P.; Jonne, N.; Sebastian, T.; Jari, T.; Steffen, N.; Petri, V. Laser cladding with coaxial wire feeding. In *International Congress on Applications of Lasers & Electro-Optics, Proceedings of the ICALEO®2012: 31st International Congress on Laser Materials Processing, Laser Microprocessing and Nanomanufacturing, Anaheim, CA, USA, 23–27 September 2012*; Laser Institute of America: Orlando, FL, USA, 2012; pp. 1196–1201. ISBN 978-0-91203-596-3.
16. Chen, Y.; Chen, X.; Jiang, M.; Lei, Z.; Wang, Z.; Liang, J.; Wu, S.; Ma, S.; Jiang, N.; Chen, Y. Coaxial laser metal wire deposition of Ti6Al4V alloy: Process, microstructure and mechanical properties. *J. Mater. Res. Technol.* **2022**, *20*, 2578–2590. [[CrossRef](#)]
17. Ji, S.; Liu, F.; Shi, T.; Fu, G.; Shi, S. Effects of Defocus Distance on Three-Beam Laser Internal Coaxial Wire Cladding. *Chin. J. Mech. Eng.* **2021**, *34*, 45. [[CrossRef](#)]
18. Zapata, A.; Bernauer, C.; Stadter, C.; Kolb, C.G.; Zaeh, M.F. Investigation on the Cause-Effect Relationships between the Process Parameters and the Resulting Geometric Properties for Wire-Based Coaxial Laser Metal Deposition. *Metals* **2022**, *12*, 455. [[CrossRef](#)]
19. Shakhverdova, I.; Nowotny, S.; Thieme, S.; Kubisch, F.; Beyer, E.; Leyens, C. Coaxial Laser Wire Deposition. *J. Phys. Conf. Ser.* **2018**, *1109*, 12026. [[CrossRef](#)]
20. Tuominen, J.; Näkki, J.; Pajukoski, H.; Hyvärinen, L.; Vuoristo, P. Microstructural and abrasion wear characteristics of laser-clad tool steel coatings. *Surf. Eng.* **2016**, *32*, 923–933. [[CrossRef](#)]
21. Ur Rahman, N.; Capuano, L.; van der Meer, A.; de Rooij, M.B.; Matthews, D.T.A.; Walmag, G.; Sinnaeve, M.; Garcia-Junceda, A.; Castillo, M.; Römer, G.R.B.E. Development and characterization of multilayer laser clad high speed steels. *Addit. Manuf.* **2018**, *24*, 76–85. [[CrossRef](#)]
22. Rahman, N.U.; Capuano, L.; de Rooij, M.B.; Matthews, D.T.A.; Garcia-Junceda, A.; Mekicha, M.A.; Cordova, L.; Walmag, G.; Sinnaeve, M.; Römer, G.R.B.E. Laser metal deposition of vanadium-rich high speed steel: Microstructural and high temperature wear characterization. *Surf. Coat. Technol.* **2019**, *364*, 115–126. [[CrossRef](#)]
23. Shi, C.; Yu, A.; Wu, J.; Niu, W.; He, Y.; Hong, X.; Shang, Q. Study on position of laser clad chip breaking dot on rake face of HSS turning tool. *Int. J. Mach. Tools Manuf.* **2017**, *122*, 132–148. [[CrossRef](#)]
24. *EN ISO 4957:1999*; Tool Steels. European Committee for Standardization: Brussels, Belgium, 1999.
25. Voestalpine BÖHLER Edelstahl GmbH & Co KG. S390-Microclean Datasheet. Available online: https://www.bohler-edelstahl.com/app/uploads/sites/92/2023/07/productdb/api/s390-microclean_en.pdf (accessed on 21 July 2023).
26. Park, G.-W.; Shin, S.; Kim, J.-Y.; Koo, Y.-M.; Lee, W.; Lee, K.-A.; Park, S.S.; Jeon, J.B. Analysis of solidification microstructure and cracking mechanism of a matrix high-speed steel deposited using directed-energy deposition. *J. Alloys Compd.* **2022**, *907*, 164523. [[CrossRef](#)]

Disclaimer/Publisher's Note: The statements, opinions and data contained in all publications are solely those of the individual author(s) and contributor(s) and not of MDPI and/or the editor(s). MDPI and/or the editor(s) disclaim responsibility for any injury to people or property resulting from any ideas, methods, instructions or products referred to in the content.